A Coupled Molecular Dynamics and XANES Data Analysis Investigation of Aqueous Cadmium(II)

ARTICLE *in* THE JOURNAL OF PHYSICAL CHEMISTRY A · NOVEMBER 2008

Impact Factor: 2.69 · DOI: 10.1021/jp806098r · Source: PubMed

4 AUTHORS, INCLUDING:

Valentina Migliorati
Sapienza University of Rome
39 PUBLICATIONS **512** CITATIONS
SEE PROFILE

Giordano Mancini
Scuola Normale Superiore di Pisa
56 PUBLICATIONS **529** CITATIONS
SEE PROFILE

Giovanni Chillemi
Cineca
105 PUBLICATIONS **1,735** CITATIONS
SEE PROFILE

A Coupled Molecular Dynamics and XANES Data Analysis Investigation of Aqueous Cadmium(II)

Paola D'Angelo,*,† Valentina Migliorati,† Giordano Mancini,†,‡ and Giovanni Chillemi*,‡

Dipartimento di Chimica, Università di Roma "La Sapienza", P. le A. Moro 5, 00185 Roma, Italy, and CASPUR, Inter-University Consortium for Supercomputing in Research, via dei Tizii 6b, 00185 Roma, Italy

Received: July 10, 2008; Revised Manuscript Received: September 4, 2008

The flexible nature of the first hydration shell of the cadmium(II) ion has been definitively assessed through an extensive study, combining X-ray absorption near-edge structure (XANES) spectroscopy and molecular dynamics (MD) simulations. The structural and dynamic properties of the cadmium(II) hydration shell have been determined from long-time MD simulations, and the influence of water−water interactions has been evaluated using the SPC/E and TIP5P water models. Comparison of the theoretical results with EXAFS data suggests that the TIP5P simulation provides a better description of the cadmium(II) hydration properties. XANES spectra have been computed starting from MD trajectories, without carrying out any minimization in the structural parameter space. The octahedral solvation of cadmium(II) in aqueous solution cannot be reconciled with the XANES results, while a flexible hydration shell is fully consistent with the experimental data, which unambiguously show the presence of a dominant percentage of heptahydrated species.

1. Introduction

Cadmium is one of the most important heavy-metal environmental toxicants. Although the overt toxic effects of this metal have been fairly well characterized, the specific mechanisms underlying many of these effects have yet to be elucidated.[1] Cadmium alters a wide variety of cellular and biochemical processes due to its ability to replace zinc(II) and calcium(II) in enzymes, proteins, and nucleic acids.[2] Structural information on cadmium(II) hydration complexes is key for understanding cadmium transport in aqueous environments and its interaction with biological molecules and proteins. In particular, it is very important to resolve the ability of cadmium(II) to mimic ions in water to adopt very different hydration geometries since this property leads to cadmium uptake and toxicity.[3]

The structure of the hydrated cadmium(II) ion in aqueous solution has been the subject of several X-ray diffraction investigations, where the number of nearest neighbors was assumed to be six and which led to consistent values for the Cd−O internuclear distance.[4] Conversely, a recent investigation combining molecular dynamics (MD) simulations, EXAFS, and large-angle X-ray scattering measurements has suggested a more dynamical picture with a first coordination shell which transits between hexa- and heptahydrated clusters.[5,6] The existence of such a flexible hydration structure could provide a rationale for the ability of cadmium(II) to substitute ions having variable coordination geometries in biological systems. Nevertheless, this finding is still controversial since a recent investigation on the hydration structure of cadmium by ab initio calculations concluded that the hexacoordinated model is more probable.[7] These new results suggest the need for additional experimental and theoretical work to support the claim that cadmium has a variable coordination number in which a heptacoordinated species plays a predominant role.

We therefore decided to reexamine our previous results[5,6] using a new and very effective experimental approach which exploits the ability of the X-ray absorption near-edge structure (XANES) spectroscopy to provide detailed information on the geometric environment of the absorbing atom.[8] X-ray absorption spectroscopy, in particular EXAFS, is a powerful experimental technique for local structure determination, which has been applied to a large variety of scientific fields. Nevertheless, in the case of aqueous solutions, while the determination of the ion−water first-shell distance is very accurate, the uncertainty in the coordination numbers is usually too large for a conclusive determination of the geometry of hydration complexes.[9−11] Conversely, a quantitative analysis of the XANES, which includes the rising edge and about 200 eV above it, can provide accurate geometrical information on the different species existing in water.[12−16] In the case of ionic solutions, the XANES spectra have been usually computed by reducing the system to a single structure since the contribution from molecules and arrangements instantaneously distorted cannot be calculated using the standard data analysis methods.[12,13] A promising strategy to overcome this problem is to analyze the XANES spectra using a microscopic description of the system derived from MD simulations. This approach has been successfully used for the analysis of cations such as nickel(II),[14] cromium(III),[15] and mercury(II).[16]

The aim of this paper is to provide a definitive picture of the structural and dynamic properties of the cadmium(II) hydration structure. To this end, we have carried out a thorough analysis of two MD simulations using two of the most widespread water models, namely, SPC/E[17] and TIP5P.[18] This procedure has highlighted the influence of the water−water interaction on the structural and dynamic properties of the cadmium(II) hydration shells. Comparison of the theoretical results with the EXAFS experimental data has allowed us to further assess the reliability of the MD simulations. Moreover, we have carried out a quantitative analysis of the XANES spectrum starting from a representative set of geometries extracted from MD calculations, without carrying out any minimization of the structural param-

* To whom correspondence should be addressed. E-mail: p.dangelo@caspur.it. Fax: +39-06-49913751 (P.D.A); E-mail: chillemi@caspur.it (G.C.).
† Università di Roma "La Sapienza".
‡ Inter-University Consortium for Supercomputing in Research.

10.1021/jp806098r CCC: $40.75
Published on Web 10/24/2008

eters. This analysis has provided a definitive experimental proof of the flexible nature of the cadmium(II) hydration shell.

2. Experimental Section

2.1. Molecular Dynamics Simulations. MD simulations of the cadmium(II) ion in aqueous solution have been performed using an effective two-body potential obtained by fitting the parameters of a suitable analytical function on an ab initio potential energy function (PES) as described in ref 6. The ab initio PES was generated taking into account scalar relativistic effects using a suitable effective core potential and including many-body effects by means of the polarizable continuum model (PCM).[19] A thorough description of the procedure used to obtain the ab initio potential energy function can be found in ref 6. Both the SPC/E[17] and TIP5P[18] water models have been employed in the MD simulations. For the SPC/E water model, we have used in the simulation the following cadmium(II)−H_2O two-body potential:

$$V(r) = \frac{q_i q_o}{r_{io}} + \frac{A_o}{r_{io}^4} + \frac{B_o}{r_{io}^6} + \frac{C_o}{r_{io}^8} + \frac{D_o}{r_{io}^{12}} + E_o e^{-F_o r_{io}} + \sum_{ih=ih1,ih2} \frac{q_i q_h}{r_{ih}} + \frac{A_h}{r_{ih}^4} + \frac{B_h}{r_{ih}^6} + \frac{C_h}{r_{ih}^8} + \frac{D_h}{r_{ih}^{12}} \quad (1)$$

where r_{io}, r_{ih1}, and r_{ih2} are the ion−water distances, and q_i, q_o, and q_h are the electrostatic charges of cadmium, oxygen, and hydrogen in the SPC/E water model, respectively (2.0, −0.8476, and 0.4238 au). A_o,..., F_o and A_h,..., D_h are the parameters obtained by the fitting procedure. In the case of the TIP5P simulation, since the TIP5P water model has two negative charges centered on two dummy atoms, the potential energy function has been adapted to the following form:

$$V(r) = \frac{A_o}{r_{io}^4} + \frac{B_o}{r_{io}^6} + \frac{C_o}{r_{io}^8} + \frac{D_o}{r_{io}^{12}} + E_o e^{-F_o r_{io}} + \sum_{ih=ih1,ih2} \frac{q_i q_h}{r_{ih}} + \frac{A_h}{r_{ih}^4} + \frac{B_h}{r_{ih}^6} + \frac{C_h}{r_{ih}^8} + \sum_{iL=iL1,iL2} \frac{q_i q_L}{r_{iL}} + \frac{A_L}{r_{iL}^4} + \frac{B_L}{r_{iL}^6} + \frac{C_L}{r_{iL}^8} \quad (2)$$

where r_{io}, r_{ih}, and r_{iL} are the ion−oxygen, ion−hydrogen, and ion−dummy atom distances, respectively, while q_i, q_h, and q_L are the atomic charges of the cadmium(II), H, and dummy atoms, respectively (2.0, 0.241, and −0.241 au). A_o,..., F_o, A_h,..., C_h, and A_L,..., C_L are the unknown parameters. All of the cadmium−SPC/E water and cadmium−TIP5P water interaction parameters obtained by the fitting procedure are reported in Table 1 of ref 6.

The simulations were carried out using the GROMACS package, version 3.2.1,[20] modified in order to include the two effective pair potentials. The system was composed of 1 cadmium(II) ion and 819 water molecules in a cubic box, using periodic boundary conditions. The system has been simulated in a NVT ensemble, where the temperature was kept fixed at 300 K using the Berendsen method[21] with a coupling constant of 0.1 ps. A cutoff of 9 Å has been used for the nonbonded interactions, using the particle Ewald method to correct the long-range electrostatic effects.[22] The simulations have been carried out for 105 ns, with a time step of 1 fs. The first 5 ns have been utilized to equilibrate the system and discarded in the following analyses.

2.2. Structural and Dynamic Analysis from MD Simulations. The structural properties of the cadmium(II) aqueous solution are described in terms of radial distribution functions, $g_{Cd-O}(r)$ and $g_{Cd-H}(r)$

$$g_{AB}(r) = \frac{\langle \rho_B(r) \rangle}{\langle \rho_B \rangle_{local}} = \frac{1}{N_A \langle \rho_B \rangle_{local}} \sum_{i \in A}^{N_A} \sum_{i \in B}^{N_B} \frac{\delta(r_{ij} - r)}{4\pi r^2} \quad (3)$$

where $\langle \rho_B(r) \rangle$ is the particle density of type B at distance r around type A, and $\langle \rho_B \rangle_{local}$ is the particle density of type B averaged over all spheres around particle A with radius r_{max} (half of the box length).

Angular distribution functions have been calculated for three different angles, the angle formed by two different Cd−O vectors in the first shell (labeled as ψ), the angle formed by the water molecule dipole vector and the Cd−O vector direction (called the tilt angle and labeled as ϕ), and the angle formed by the normal to the water plane and the Cd−O vector direction (labeled as ζ).

To describe the distribution of water molecules around the cadmium(II) ion, axial−radial 2D density maps (cylindrical distribution functions) have been calculated.[23] These maps show the distribution of water oxygen atoms with respect to the chosen reference axis containing the ion and the oxygen atom of a selected water molecule.

The cadmium(II) diffusion coefficient, D_{Cd}, has been evaluated using two different methods. In the first approach, D_{Cd} has been determined from the mean square displacement (MSD) using the Einstein relation[23]

$$D_{Cd} = \frac{1}{6} \lim_{t \to \infty} \frac{\langle ||\mathbf{r}_{Cd}(t) - \mathbf{r}_{Cd}(0)||^2 \rangle}{t} \quad (4)$$

where $\mathbf{r}_{Cd}(0)$ is the cadmium(II) initial position and $\mathbf{r}_{Cd}(t)$ is the position of the ion at time t. In the second method, we have calculated the normalized velocity autocorrelation function (VACF), $C(t)$, defined as

$$C(t) = \frac{\langle \mathbf{v}_{Cd}(t) \mathbf{v}_{Cd}(0) \rangle}{\langle \mathbf{v}_{Cd}(0)^2 \rangle} \quad (5)$$

where $\mathbf{v}_{Cd}(t)$ and $\mathbf{v}_{Cd}(0)$ are the velocities of the ion at times t and zero, respectively.

The cadmium(II) diffusion coefficient has been calculated from $C(t)$ by the Green−Kubo formula

$$D_{Cd} = \frac{k_B T}{m_{Cd}} \int_0^\infty C(t) dt \quad (6)$$

where k_B is the Boltzmann constant, T is the temperature, and m_{Cd} the mass of the cadmium(II) ion.

The radial and angular distribution functions have been generated using in-house-written codes, while 2D density maps and diffusion coefficients have been obtained using GROMACS analysis tools (g_densmap for the density maps, and g_msd and g_velacc for MSD and VACF calculations, respectively).[23]

2.3. X-ray Absorption Measurements. A 0.1 M cadmium(II) water solution was prepared by dissolving the appropriate amount of $Cd(NO_3)_2 \cdot 4H_2O$ in freshly distilled water and adding HNO_3 in order to prevent hydrolysis. Cd K-edge X-ray absorption spectra were obtained using the EMBL spectrometer at DESY.[24] Spectra were recorded in transmission mode using a Si(311) double-crystal monochromator detuned to 30% for harmonic rejection.[25] Data points were collected for 1 s each, and three spectra were recorded and averaged after performing an absolute energy calibration.[26] The DORIS III storage ring was running at an energy of 4.4 GeV with positron currents between 70 and 40 mA. The solution was kept in a cell with Kapton film windows and a Teflon spacer of 3 mm.

2.4. EXAFS Data Analysis. In the standard EXAFS analysis of disordered systems, only two-body distributions are included, and the $\chi(k)$ signal is represented by the equation

$$\chi(k) = \int_0^\infty \mathrm{d}r\, 4\pi\rho r^2 g(r) A(k,r) \sin[2kr + \phi(k,r)] \qquad (7)$$

where $A(k,r)$ and $\phi(k,r)$ are the amplitude and phase functions, respectively, and ρ is the density of the scattering atoms. $\chi(k)$ theoretical signals can be calculated by introducing into eq 7 the model radial distribution functions obtained from MD simulations. Both the Cd−O and Cd−H $g(r)$'s obtained from the two simulations have been used to calculate the single scattering first-shell $\chi(k)$ theoretical signal, as the ion−hydrogen interactions have been found to provide a detectable contribution to the EXAFS spectra of several metal ions in aqueous solutions.[9−12] Comparison of the theoretical and experimental total $\chi(k)$ signals allows the reliability of the $g(r)$'s and consequently of the theoretical scheme and the water model used in the simulations, which is to be checked.

The EXAFS theoretical signals have been calculated by means of the GNXAS program, and a thorough description of the theoretical framework for the multiple scattering analysis can be found in ref 27. Phase shifts, $A(k,r)$ and $\phi(k,r)$, have been calculated starting from one of the TIP5P configurations by using muffin-tin potentials and advanced models for the exchange−correlation self-energy (Hedin−Lundqvist).[28] The values of the muffin-tin radii are 0.2, 0.9, and 1.4 Å for hydrogen, oxygen, and cadmium, respectively. Inelastic losses of the photoelectron in the final state have been accounted for intrinsically by a complex potential. The imaginary part also includes a constant factor accounting for the core−hole width.

2.5. XANES Data Analysis and Computational Procedure. The XANES spectrum of cadmium(II) in aqueous solution has been analyzed starting from the microscopic description of the system derived from the TIP5P and SPC/E simulations. The XANES spectra at high energies are strongly broadened by the core−hole width, and the structural and electronic details are smeared out from the spectra (the energy of the Cd K-edge is 26711 eV and the core−hole width is 7.28 eV).[29] Recently, suggestions to apply core−hole width deconvolution methods to analyze X-ray absorption spectra have appeared in the literature[30] as this treatment largely facilitates the detection of spectral features and the comparison with theoretical calculations. This procedure has been previously applied by Kodre at al.[31] to unveil the presence of multielectron photoexcitations in the K-edge absorption spectrum of Cd vapor and in the XANES analysis of mercury(II) in aqueous solution.[13,16] Also, in the present case, the Cd K-edge raw experimental data have been deconvolved of the whole tabulated core−hole width and a Gaussian filter with full width at half-maximum of about 3 eV has been applied. The comparison between the raw and the deconvolved spectra is shown in Figure 1S in the Supporting Information. It is important to underline that even if in principle the deconvolution procedure could introduce small distortions in the experimental data, the advantage of this approach is to avoid the use of the phenomenological broadening function $\Gamma(E)$ in the calculation of the theoretical spectrum to mimic electronic damping. This method is known to be a shortcoming in the XANES analysis, and the deconvolution procedure allows one to overcome, at least partially, this problem.

In the first step, the XANES spectrum associated with the MD trajectories has been calculated with the MXAN program[32] using only the real part of the HL potential, that is, theoretical spectra do not account for any intrinsic and extrinsic inelastic process, while the damping associated with the experimental resolution is accounted for by convolution with a Gaussian function with a full width at half-maximum of 3 eV.

In the second step, a minimization in the nonstructural parameter space has been carried out to perform a comparison with the experimental data. In particular, the inelastic processes are accounted for by convolution with a broadening Lorentzian function having an energy-dependent width of the form $\Gamma(E) = \Gamma_c + \Gamma_{mfp}(E)$. The constant part Γ_c accounts for the core−hole lifetime, and it has not been included in our calculations as it has been removed from the experimental data, while the energy-dependent term represents all of the intrinsic and extrinsic inelastic processes.[32] The $\Gamma_{mfp}(E)$ function is zero below an energy onset of E_s (which, in extended systems, corresponds to the plasmon excitation energy) and starts increasing from a given value A, following the universal functional form of the mean free path in solids.[33] Both the onset energy E_s and the jump A are introduced in the $\Gamma_{mfp}(E)$ function via an arctangent functional form to avoid discontinuities.

Least-squares fits of the XANES experimental data have been performed by minimizing the R_{sq} function defined as

$$R_{sq}(\{\lambda\}) = \sum_{i=1}^{N} [\alpha_{exp}(E_i) - \alpha_{mod}(E_i;\lambda_1, \lambda_2, ..., \lambda_p)]^2 \times W(E_i) \qquad (8)$$

where N is the number of experimental points E_i, $\{\lambda\} = (\lambda_1, \lambda_2, ..., \lambda_p)$ are the p parameters to be refined, and $W(E_i)$ is a weight function.[32]

Previous investigation on nickel(II) and mercury(II) in water have shown that the second hydration shell provides a detectable contribution to the XANES spectrum of these systems.[14,16] For this reason, in the present XANES calculation, we have included both the first and second hydration shells in the analysis. In particular, we have considered all of the water molecules separated from the cadmium(II) ion by a distance shorter than 5.2 Å since water molecules at larger distance have been found to provide a negligible contribution.

Two trajectories containing the cadmium(II) ion and its first two hydration shells have been extracted from the total simulation in different time ranges when the ion was six- and seven-coordinated. As a result, the former trajectory contained first-shell hexahydrated clusters only, while the latter contained first-shell heptacoordinated clusters. From each trajectory we extracted 100 snapshots saved every 30 ps. Each snapshot has been used to generate the XANES spectrum associated with the corresponding instantaneous geometry, and the averaged theoretical spectrum has been obtained by summing all of the spectra and dividing by the total number of MD snapshots used. As previously mentioned, at this stage, only the real part of the HL potential has been used, that is, theoretical spectra do not account for any intrinsic and extrinsic inelastic process. An IBM SP5 (168× PW5@1.9 GHz) parallel machine has been used, and the execution time for a single MXAN calculation on eight CPUs was 2.1 min.

An important question when dealing with the computation of spectra from MD simulations is to determine the total sampling length that is necessary to have a statistically significant average. To this end, we have carried out, for each averaged theoretical spectrum, a statistical treatment of the data. In particular, we have calculated a residual function defined as

$$\mathrm{RMS} = \sqrt{\sum_i [\alpha^N(E_i) - \alpha^{N-1}(E_i)]^2} \qquad (9)$$

where $\alpha^N(E_i)$ is the theoretical spectrum averaged over N snapshots and the sum is extended over all of the energy points

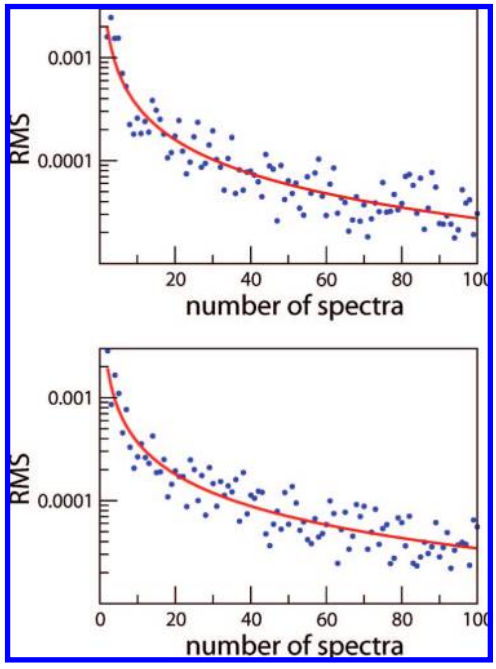

Figure 1. Residual function RMS of the XANES averaged spectra as a function of the number of MD snapshots for hexa- (upper panel) and hepta- (lower panel) coordinated first-shell clusters.

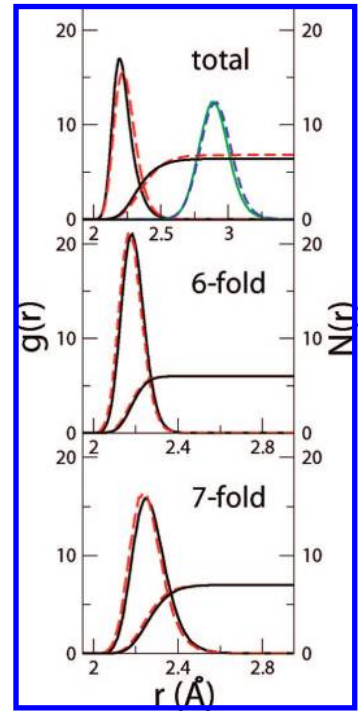

Figure 2. Top panel: TIP5P (dashed red line) and SPC/E (black solid line) Cd−O $g(r)$'s calculated on the total trajectories and corresponding running integration numbers. TIP5P (dashed blue line) and SPC/E (green solid line) Cd−H $g(r)$'s. Middle panel: TIP5P (dashed red line) and SPC/E (black solid line) Cd−O $g(r)$'s calculated on hexacoordinated simulation frames and corresponding running integration numbers. Bottom panel: TIP5P (dashed red line) and SPC/E (black solid line) Cd−O $g(r)$'s calculated on heptacoordinated simulation frames and corresponding running integration numbers.

E_i. A residual value of 10^{-4} was chosen to establish the number of spectra which is necessary to have a statistically significant average. The results of this analysis for the TIP5P simulation are shown in Figure 1, where the RMS function is plotted against the number of averaged spectra for the hexa- and heptacoordinated first-shell clusters (upper and lower panels, respectively). As evident from the plots, 100 configurations are enough to reach convergence in both cases. The results obtained from the SPC/E simulations are very similar, and they are not shown for the sake of brevity.

3. Results and Discussion

3.1. Hydration Structure from MD Simulations. An accurate description of the structural and dynamical properties of the cadmium(II) aqueous solution has been gained by a thorough analysis of the SPC/E and TIP5P simulations previously published by our group.[6] Both simulations started from a hexacoordinated first-shell configuration around the cadmium(II) ion, and after an induction time of 230 and 155 ps for the SPC/E and TIP5P models, respectively, the system went to heptacoordination. In both cases, a very flexible cadmium(II) ion first hydration shell was detected, which transits among coordination numbers of six, seven, and, for relatively short times, eight. In particular, in the SPC/E trajectory, the cadmium(II)$-(H_2O)_6$, cadmium(II)$-(H_2O)_7$, and cadmium(II)$-(H_2O)_8$ clusters are present for 65.0, 34.9, and 0.1% of the simulation time, respectively, with corresponding longest lifetimes of 2297, 1048, and 10 ps. In the TIP5P case, the six-, seven-, and eight-coordinated complexes are detected for 17.5, 81.7, and 0.8% of the time, respectively, with longest lifetimes of 220, 815, and 15 ps.[6] The different dynamical behavior between the two simulations is due to the relative higher openness of the TIP5P model, which gives rise to a larger number of exchange events between six- and seven-coordinated complexes and increases the stability of the heptahydrated species as compared to that of the hexahydrated ones.

Structural arrangements of water molecules around cadmium(II) are investigated by computing the Cd−O and Cd−H radial distribution functions, and the results are collected in Figure 2. The TIP5P Cd−O first-shell maximum is shifted toward larger distances as compared to the SPC/E peak (the first peak distances are 2.25 and 2.22 Å for TIP5P and SPC/E, respectively). Moreover, the average coordination numbers of the hydrated cadmium(II) ion are 6.8 and 6.3 for the TIP5P and SPC/E calculations, respectively, indicating that in the former case, the heptacoordinated cluster is the dominant species, while in the latter, the octahedral complex is present most of the simulation time.

To get a deeper insight into the different behavior originating from the two water models, we have separately analyzed the MD configurations in which either the hexa- or the heptahydrated species are present. The corresponding Cd−O radial distribution functions are shown in Figure 2. In particular, the comparison between the TIP5P and SPC/E $g(r)$'s associated with the hexacoordinated complexes is shown in the middle panel of Figure 2. The Cd−O $g(r)$ first-peak maxima are almost coincident, showing that the geometry of the octahedral complexes is the same in both simulations. A similar result has been obtained for the heptahydrated cluster (bottom panel of Figure 2), which has a longer Cd−O first- shell distance as compared to that of the hexacoordinated one. The full list of structural parameters describing all of the $g(r)$'s is reported in Table 1S of the Supporting Information. As a consequence, the geometry of the cadmium(II)$-(H_2O)_6$ and cadmium(II)$-(H_2O)_7$ clusters is the same regardless the water model used in the simulation, and the differences of the first-peak position of the total TIP5P and SPC/E $g(r)$'s is only due to the different percentages of hexa- and heptacoordinated complexes occurring in the simulations.

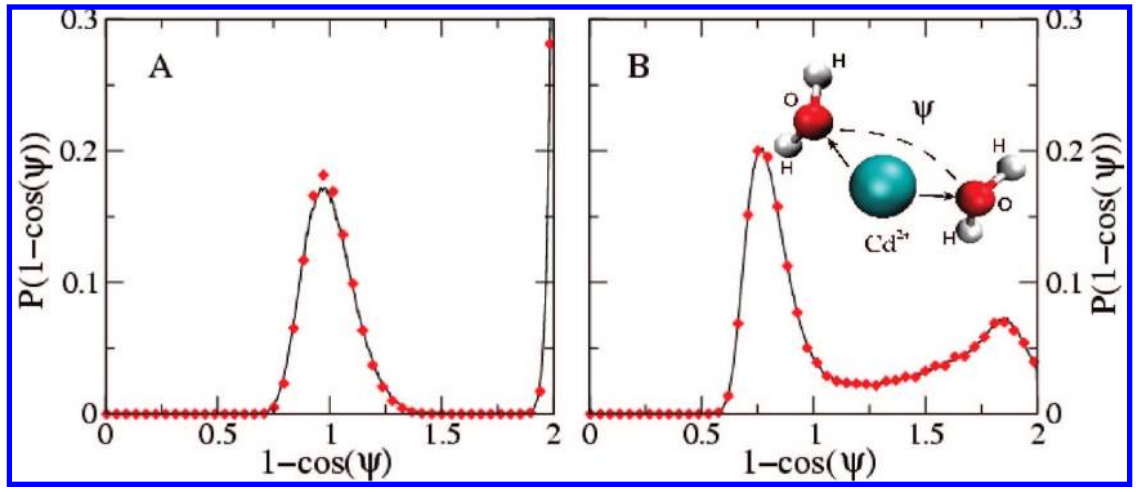

Figure 3. O−Cd−O (ψ) angular distribution functions (a.d.f.) calculated from the TIP5P and SPC/E trajectories (black solid line and red dotted line, respectively). (A) The a.d.f. calculated from hexacoordinated first-shell structures. (B) The a.d.f. calculated from heptacoordinated first-shell structures.

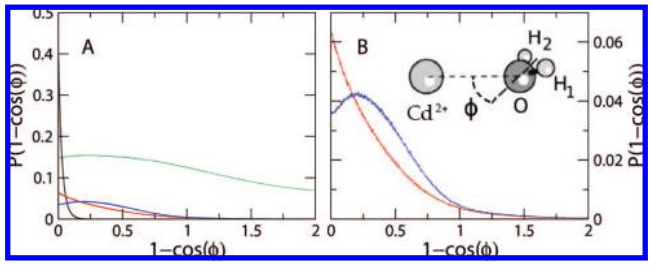

Figure 4. Tilt angle (ϕ) angular distribution functions (a.d.f). (A) The a.d.f calculated for the TIP5P first hydration shell (black line), TIP5P and SPC/E second hydration shells (blue and red lines, respectively), and TIP5P bulk water (green line). (B) The a.d.f. calculated for the TIP5P and SPC/E second hydration shell (blue and red lines, respectively).

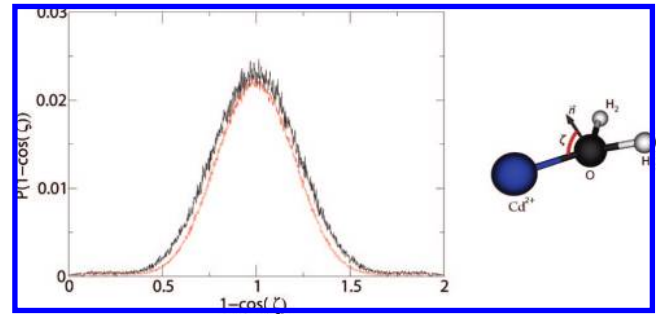

Figure 5. ζ angular distribution function calculated from the TIP5P trajectory for hexa- and heptacoordinated first-shell structures (red and black lines, respectively).

A further proof of this finding has been gained by looking at the geometrical arrangement of the first-shell water molecules around the cadmium(II) ion for the six- and seven-coordinated complexes, obtained from the angular distribution functions (a.d.f.) of the ψ and ϕ angles plotted as a function of $1 - \cos(x)$ ($x = \psi, \phi$). Figure 3 shows the ψ angular distribution function for the hexa- and heptacoordinated cluster (panels A and B, respectively) obtained from the TIP5P and SPC/E simulations. The two simulations give identical results, and the six-coordinated cluster maxima are located at $1 - \cos(x) = 1$ and $1 - \cos(x) = 2$, corresponding to ψ values of 90° and 180°, as expected for an octahedral hydration complex. The peak maxima for the seven-coordinated cluster are found at ψ values of about 75° and 145°, which are very close to the O−Cd−O angles obtained for the stable minimum at C_2 symmetry from ab initio calculations of the cadmium(II)−$(H_2O)_7$ cluster.[6]

Figure 4 shows the ϕ a.d.f. calculated for first and second hydration shells and bulk water. As far as the first hydration shell is concerned, identical distributions are obtained from the two simulations, and only the TIP5P one has been reported for the sake of brevity (panel A of Figure 4). The most probable value of ϕ for the first hydration shell is 0°, corresponding to a water dipole moment vector oriented along the Cd−O direction. The ϕ distribution for the first shell drops to zero for $\phi \approx 35°$, at slightly bigger angles than first-row transition-metal ions such as zinc(II) and nickel(II), for which the ϕ distribution becomes 0 at 30°.[34] Therefore, the first-shell water molecules of the cadmium(II) ion are slightly more free to rotate as compared to the water molecules of the octahedral complexes. In the case of the second shell (panel B of Figure 4), two different preferred orientations are obtained; the SPC/E distribution function peak is found at $\phi = 0°$, while the TIP5P ϕ distribution function has a well-defined maximum at $\phi = 36°$. This effect is caused by the geometry of the TIP5P water model, which, having five atoms and being more bulky than SPC/E, does not allow the water molecules to be oriented along the Cd−O direction. Both ϕ distributions drop to 0 at $\phi \approx 100°$, a much bigger angle than that of the first shell, indicating less tightly oriented water molecules. At longer distances, up to 10 Å, no preferred orientation can be observed. Since, in this case, the SPC/E and TIP5P results are almost identical, only the TIP5P ϕ distribution function has been reported in Figure 4 (panel A, green line).

As it is not possible to establish whether a water molecule is rotating in its plane or is really tilted using only the ϕ angle distribution, the ζ angular distribution function has been calculated for the first six- and seven-fold coordinated shell (see Figure 5). As all of the remaining MD analyses reported in this paragraph produced the same results for the two water models, hereafter, we will show only those of the TIP5P model. The distribution peak is found at $\zeta \approx 90°$ for both hexa- and heptacoordinated clusters, indicating that the Cd−O vector is located most of the time in the water molecule plane, with maximum deviations of 30° above and below the plane (the ζ distribution, in fact, drops to 0 at $\zeta \approx 60$ and 120°). Moreover, the curve associated with the seven-coordinated frames (black line) is slightly broader since, in this case, the water molecule dipole is more free to rotate.

The flexibility of the cadmium(II) first hydration shell can be highlighted using axial−radial 2D density maps for the hexa-

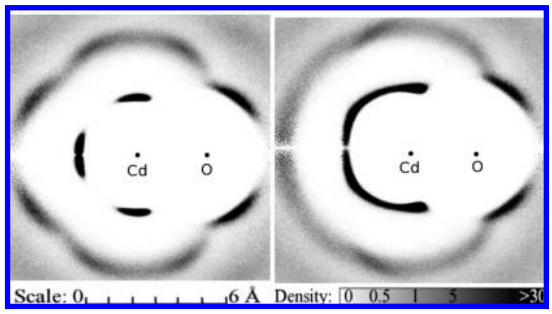

Figure 6. Axial−radial 2D density map of water molecules around a fixed Cd−O axis for the TIP5P simulation. Left panel: Oxygen distribution function calculated from hexacoordinated frames. Right panel: Oxygen distribution function calculated from heptacoordinated frames.

and heptacoordinated complexes (left and right panels of Figure 6, respectively). The map obtained for the six-fold coordinated shell is typical of an octahedral cluster, such as that obtained for the nickel(II) hydration shell.[35] On the contrary, in the case of the heptahydrated cluster, the oxygen atoms give rise to a uniform distribution around the chosen axis, showing the higher mobility of the first-shell water molecules.

All together, these results reinforce the finding that the water model does not affect the first-shell hexa- and heptahydrated complex structures, while the higher flexibility of the TIP5P model modifies the dynamical behavior of the system.

To get a deeper insight into the dynamic properties of the cadmium(II) ion in aqueous solution, we have calculated the cadmium(II) diffusion coefficient using velocity autocorrelation functions (VACF) and mean square displacement (MSD) methods. The calculated and experimental ion diffusion coefficients are listed in Table 1. In both simulations, the diffusion coefficients estimated from the MSD and the VACF match quite well, but a better agreement with the experimental value[36]is found for the TIP5P water model. The cadmium(II) ion exhibits a faster translational dynamics in the TIP5P simulation as compared to that for the SPC/E trajectory. This result agrees well with the general picture drawn by the TIP5P simulation, characterized by a greater water mobility, resulting in shorter values of the water residence time and a greater number of water exchange events between the first hydration shell and the bulk.[6]

3.2. EXAFS Analysis. As shown in the previous sections, the TIP5P and SPC/E simulations present a difference of about 0.03 Å in the position of the Cd−O first-shell $g(r)$'s, while the geometry of the cadmium(II)−$(H_2O)_6$ and cadmium(II)−$(H_2O)_7$ clusters is the same. The $\chi(k)$ theoretical signals have been calculated using eq 7. starting from the total TIP5P and SPC/E Cd−O and Cd−H radial distribution functions. The structural parameters derived from the simulations were kept fixed during the EXAFS analysis. In this way, the first hydration shell structure obtained from the two simulations can be directly compared with the experimental data, and the validity of the theoretical results can be assessed. Note that all of the EXAFS analyses have been carried out using the raw experimental data. In the upper panels of Figure 7, the comparison between the experimental signal and the theoretical curves is reported for the TIP5P and SPC/E models (left and right panels, respectively). The $\gamma^{(n)}$ signals are shown multiplied by k^2 for better visualization. The first two curves from the top of each panel are the Cd−O and Cd−H first-shell $\gamma^{(2)}$ contributions. The

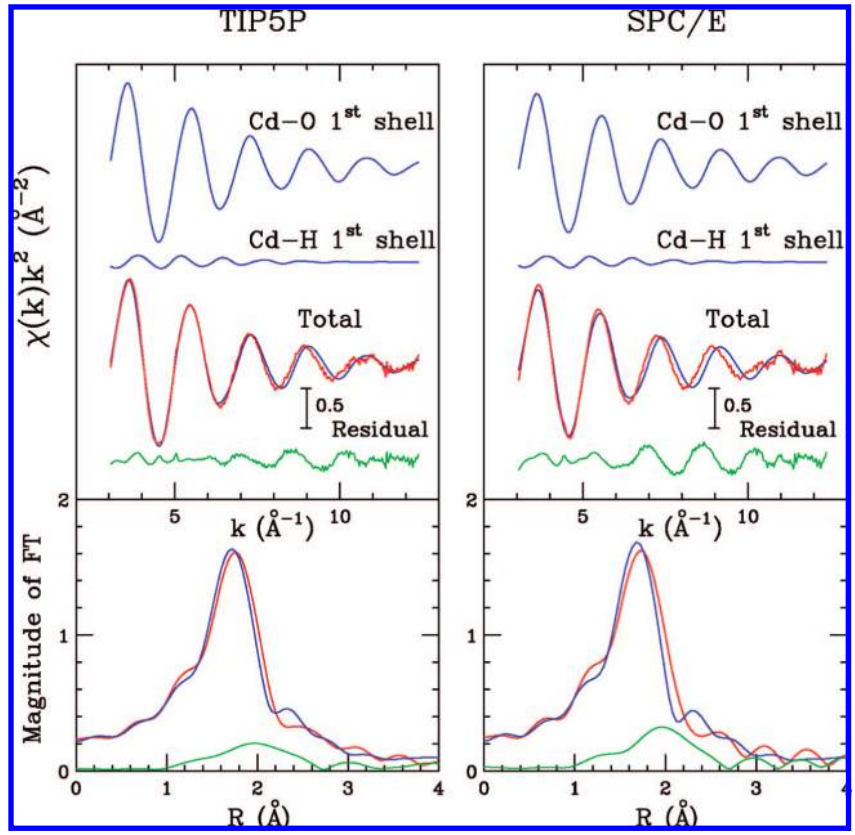

Figure 7. Upper panels: Comparison between the TIP5P and SPC/E EXAFS theoretical signals (blue line) calculated from the total Cd−O and Cd−H $g(r)$'s and raw experimental data (red line). The residual signals (green line) are also shown. Lower panels: Nonphase-shifted corrected Fourier transforms of the experimental data (red line), of the theoretical signals (blue line), and of the residual curves (green line).

reminder of the figures show the total theoretical contributions compared with the experimental spectra and the resulting residuals. As expected, the dominant contribution to the total EXAFS signal is given by the ion−O first-shell signal, and as a consequence, the EXAFS structural information is particularly accurate for the shape of the ion−O $g(r)$'s first peaks only. Overall, the calculated EXAFS spectra match the experimental data reasonably well in both cases, with R_i values of 0.466×10^{-6} and 0.147×10^{-5} for TIP5P and SPC/E, respectively (see ref 37 for the definition of this index of agreement). Therefore, the structural and dynamical information derived from the two simulations is basically correct. However, the TIP5P $\chi(k)$ theoretical signal is in better agreement with the experimental data, thus showing that this simulation provides a better description of the water structure around the cadmium(II) ion. In the SPC/E EXAFS analysis, the presence of a leading frequency can be clearly identified in the residual curve. This behavior is due to the slightly short value of the average Cd−O first-shell distance obtained from the SPC/E as compared to the experimental results. This finding is reinforced by the Fourier transform (FT) moduli of the EXAFS $\chi(k)k^2$ theoretical, experimental, and residual signals shown in the lower panels of Figure 7. The FTs have been calculated in the k range of 3.1−12.0 Å^{-1}, with no phase shift correction applied. A quite good agreement between the FTs of the theoretical and experimental signals has been found for the TIP5P simulation, while the experimental first-neighbor peak is found to be broader and shifted toward longer distances than predicted by the SPC/E simulation. This is a first indication that the EXAFS experimental data are better reproduced by a flexible hydration shell with a high percentage of heptacoordinated species.

In the second step of the analysis, we have examined the compatibility of the EXAFS spectrum with the existence of an octahedral geometry of the solvated cadmium(II) ion. To this end, we calculated the $\chi(k)$ theoretical signal associated with the hexacoordinated $g(r)$'s reported in the middle panel of Figure 2. The results are shown in Figure 8. Both the frequency and the amplitude of the theoretical curve are in poor agreement with the experimental data. In particular, the Cd−O first-shell distance of the hydrated cluster is too short, and the octahedral complex is too stiff as compared to the experimental determination. This is reflected in a different width and peak position of the FT of the $\chi(k)$ signals, as shown in the lower panel of Figure 8.

3.3. XANES Analysis. As previously mentioned, XANES is extremely sensitive to the geometric environment of the absorbing atom as multiple scattering effects make large contributions to this region of the X-ray absorption spectra. For this reason, a quantitative analysis of the XANES data could provide a definitive answer on the hydration properties of the cadmium(II) ion and, in particular, on the percentage of hexa- and heptacoordinated complexes present in aqueous solution. In the first step of the analysis, we have calculated the theoretical XANES spectra associated with the hexa- and heptahydrated complexes. To this end, we have extracted from each simulation two trajectories, the former containing first-shell hexahydrated clusters only and the latter containing first-shell heptacoordinated clusters. In both cases, also the second hydration shell was considered, including all of the water molecules up to 5.2 Å. The corresponding XANES theoretical spectra obtained from 100 MD snapshots (not including intrinsic and extrinsic inelastic processes) are shown in Figure 9. In the upper panel, we report the XANES theoretical spectra associated with the octahedral hydration structure for the TIP5P and SPC/E simulations, while

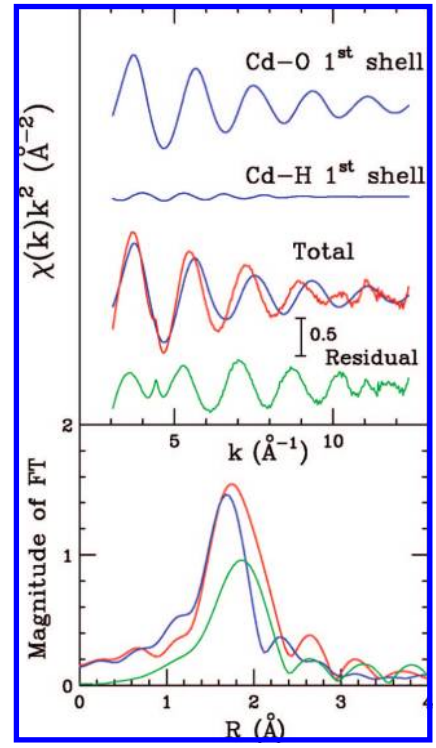

Figure 8. Upper panel: Comparison between the TIP5P EXAFS theoretical signal (blue line) calculated from the hexacoordinated Cd−O and Cd−H $g(r)$'s and raw experimental data (red line). The residual signal (green line) is also shown. Lower panel: Nonphase-shifted corrected Fourier transforms of the experimental data (red line), of the theoretical signal (blue line), and of the residual curve (green line).

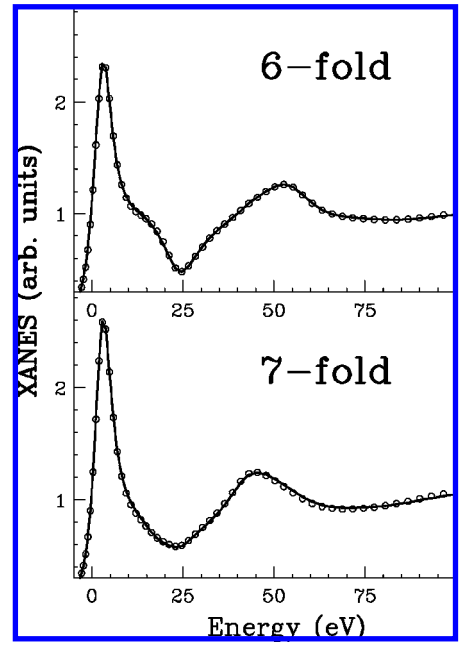

Figure 9. Upper panel: Comparison of the averaged XANES theoretical spectra of cadmium(II) in aqueous solution calculated from the TIP5P (solid line) and SPC/E (dotted line) hexacoordinated simulation frames. Lower panel: Comparison of the averaged XANES theoretical spectra of cadmium(II) in aqueous solution calculated from the TIP5P (solid line) and SPC/E (dotted line) heptacoordinated simulation frames.

the XANES theoretical spectra calculated from the heptacoordinated clusters are shown in the lower panel. The spectra

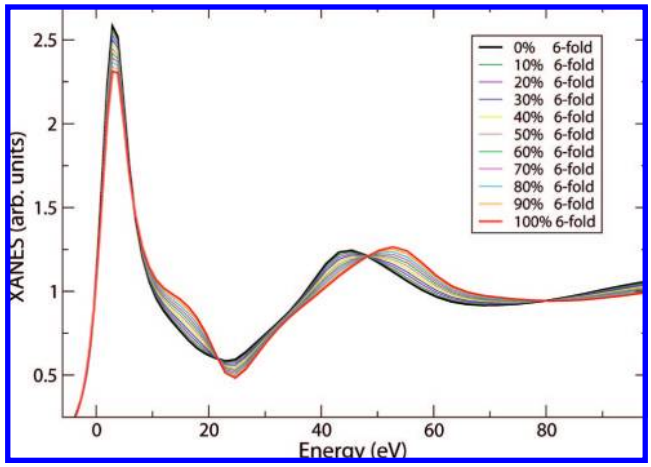

Figure 10. Averaged XANES theoretical spectra calculated with different percentages of hexa- and heptacoordinated clusters.

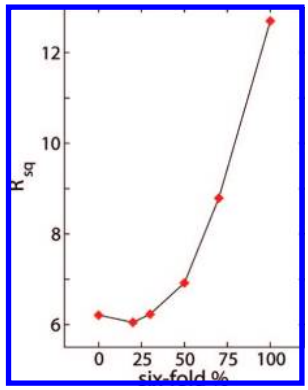

Figure 11. Goodness-of-fit (R_{sq}) versus percentage of the hexacoordinated complex of the XANES theoretical spectra.

obtained from the two simulations are identical, and therefore, in the following analysis, only the TIP5P trajectory has been used.

In the second step, we exploited the potentiality of the XANES technique to unveil the structural and dynamic properties of the cadmium(II) hydration sphere. In particular, we were interested in determining the percentage of the heptaaqua and hexaaqua ion existing in solution. To this end, we calculated several averaged theoretical spectra with variable percentages of hexa- and heptacoordinated complexes, and the obtained trend is depicted in Figure 10. The calculated XANES spectra present noticeable differences all along the energy range, showing the sensitivity of XANES to the geometry of the cadmium(II) hydration cluster. In particular, the edge intensity is lowered in the spectrum containing only the hexacoordinated complex, which exhibits a different shape in the region around 18 eV and a shift of the first maximum around 50 eV.

To determine the effective percentages of the two hydration complexes, it is necessary to compare the total averaged XANES spectra with the experimental data. To this end, all inelastic processes have been accounted for by convoluting the theoretical averaged spectra with a broadening Lorentzian function, and the corresponding E_s and A nonstructural parameters have been optimized. Note that the E_s values obtained from the minimization procedures were in the range of 8.0−9.0 eV. The agreement between the experimental and theoretical data has been assessed by the goodness-of-fit parameter (R_{sq}) as described in eq 8. In Figure 11, the R_{sq} values are plotted against the percentage of hexahydrated clusters used in the calculation of the averaged

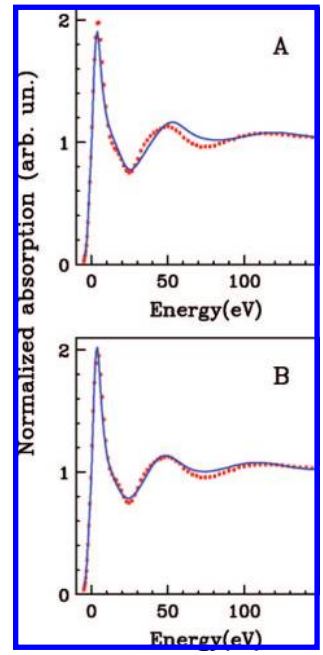

Figure 12. (A) Comparison between the averaged XANES theoretical spectrum including the hexacoordinated first-shell clusters (blue solid line) and the deconvolved experimental data (red dotted line) of cadmium(II) in aqueous solution. (B) Comparison between the averaged XANES theoretical spectrum calculated from the TIP5P trajectory with 80% of hepta- and 20% of hexacoordinated clusters (blue solid line) and the deconvolved experimental data (red dotted line).

XANES theoretical spectrum. The picture that emerges is quite informative because the lowest R_{sq} value is obtained for a hexacoordinated cluster percentage of 20%, which corresponds to the result obtained from the TIP5P simulation. Thus, this XANES analysis confirms the finding previously obtained from EXAFS, that is, the TIP5P simulation provides a very accurate description of the hydration properties of the cadmium(II) ion.

In Figure 12, the averaged theoretical spectra corresponding to hexacoordinated cluster percentage of 100 and 20% are compared with the experimental spectrum (panels A and B, respectively). In the former case, as expected, the agreement between the experimental and theoretical spectra is not very good both in the low- and high-energy regions of the spectrum. The intensity of the edge is too small, and the position of the first maximun is shifted as compared to the experimental data. Conversely, the averaged theoretical spectrum calculated from the TIP5P trajectory is in excellent agrement with the experimental data in all of the energy range (panel B of Figure 12). Small discrepancies between the theoretical and experimental spectra are found at about 20 and 70 eV from the edge. A recent investigation on the multielectron photoexcitations affecting the Cd K-edge has been carried out by Kodre et al.[31] The analysis of the Cd vapor absorption spectrum after natural-width deconvolution has revealed the presence of anomalous features in the atomic background due to multielectron excitation. In particular, the onset of the 1s4d and 1s4p multielectron transitions was found at about 20 and 70 eV, respectively, and this phenomenon could be responsible for the small discrepancies found in our MXAN analysis, which is carried out in the one-electron approximation. It is important to remark that this last XANES spectrum has been calculated from the istantaneous configurations of the TIP5P simulations, and no minimization has been carried out in the structural parameter space. Due to the high sensitivity of the XANES technique toward the structural environment of the photoabsorber, this approach is a

TABLE 1: Theoretical Diffusion Coefficients (in 10^{-5} cm^2/s) of the Cadmium(II) Ion in Aqueous Solution Calculated with the Mean Square Displacements (MSD) and Velocity Autocorrelation Functions (VACF) Methods, Compared with the Experimental Value

	MSD	VACF
SPC/E	0.68 (0.08)	0.69 (0.04)
TIP5P	0.73 (0.08)	0.71 (0.04)
experimental[a]	0.719	

[a] Ref 36.

very strict test on the quality of the potentials used in the MD simulations, and the almost perfect agreement between the averaged theoretical and experimental XANES spectra proves the reliability of the entire computational procedure.

4. Conclusion

This study provides a definitive experimental proof of the flexible nature of the cadmium(II) ion first hydration shell, which transits between coordination numbers of six and seven, with a dominant percentage of heptahydrated species. An accurate analysis of two MD simulations, carried out with the SPC/E and TIP5P water models, has highlighted that the water−water interactions do not affect the structure of the cadmium(II) ion first hydration shell but only the stability of the hexa- and heptahydrated species. Comparison of the theoretical results with EXAFS experimental data has shown that the TIP5P simulation provides a more reliable description of the cadmium(II) hydration structure. A quantitative analysis of the XANES spectra has been carried out using a microscopic description of the system derived from MD simulations. This analysis has shown that the XANES experimental spectra cannot be reproduced by a cadmium(II) octahedral solvation structure. Conversely, the experimental data are consistent with the existence of a flexible hydration shell with a high percentage of heptahydrated species (80%), in agreement with the TIP5P results.

Acknowledgment. We would like to thank CASPUR for technical support.

Supporting Information Available: Figure showing the K-edge X-ray absorption spectrum of the cadmium(II) aqueous solution before and after the deconvolution of the core−hole lifetime width. Table reporting the structural parameters of the first cadmium(II)−O $g(r)$ peaks for the TIP5P and SPC/E simulations. This material is available free of charge via the Internet at http://pubs.acs.org.

References and Notes

(1) Stohs, S. J.; Bagchi, D. *Free Radical Biol. Med.* **1995**, *18*, 321–336.
(2) Jennette, K. W. *Environ. Health Perspect.* **1981**, *40*, 233–252.
(3) Foulkes, E. C. *Exp. Biol. Med.* **2000**, *223*, 234–240.
(4) (a) Bol, W.; Gerrits, G. J. A.; van Panthaleon van Eck, C. L. *J. Appl. Crystallogr.* **1970**, *3*, 486–492. (b) Ohtaki, H.; Maeda, M.; Ito, S. *Bull. Chem. Soc. Jpn.* **1974**, *47*, 2217–2221. (c) Caminiti, R.; Johansson, G. *Acta Chem. Scand.* **1981**, *A35*, 373–381.
(5) D'Angelo, P.; Chillemi, G.; Barone, V.; Mancini, G.; Sanna, N.; Persson, I. *J. Phys. Chem. B* **2005**, *109*, 9178–9185.
(6) Chillemi, G.; Barone, V.; D'Angelo, P.; Mancini, G.; Persson, I.; Sanna, N. *J. Phys. Chem. B* **2005**, *109*, 9186–9193.
(7) Pye, C. C.; Toney, M. R.; Rudolph, W. W. *Can. J. Anal. Sci. Spectrosc.* **2006**, *51*, 140–146.
(8) Sayers, D. E.; Stern, A.; Lytle, F. W. *Phys. Rev. Lett.* **1971**, *27*, 1204–1207.
(9) D'Angelo, P.; Di Nola, A.; Filipponi, A.; Pavel, N. V.; Roccatano, D. *J. Chem. Phys.* **1994**, *100*, 985–994.
(10) D'Angelo, P.; Pavel, N. V.; Roccatano, D.; Nolting, H.-F. *Phys. Rev. B* **1996**, *54*, 12129–12138.
(11) D'Angelo, P.; De Panfilis, S.; Filipponi, A.; Persson, I. *Chem.—Eur. J.* **2008**, *14*, 3045–3055.
(12) D'Angelo, P.; Benfatto, M.; Della Longa, S.; Pavel, N. V. *Phys. Rev. B* **2002**, *66*, 064209−064215.
(13) Chillemi, G.; Mancini, G.; Sanna, N.; Barone, V.; Della.Longa, S.; Benfatto, M.; Pavel, N. V.; D'Angelo, P. *J. Am. Chem. Soc.* **2007**, *129*, 5430–5436.
(14) D'Angelo, P.; Roscioni, O. M.; Chillemi, G.; Della Longa, S.; Benfatto, M. *J. Am. Chem. Soc.* **2006**, *128*, 1853–1858.
(15) (a) Merkling, P J; Muñoz-Páez, A.; Martínez, J. M.; Pappalardo, R. R.; Sánchez Marcos, E. *Phys. Rev. B* **2001**, *64*, 092201–092209. (b) Merkling, P. J.; Muñoz-Páez, A.; Sánchez Marcos, E. *J. Am. Chem. Soc.* **2002**, *124*, 10911–10920. (c) Merkling, P J; Ayala, R.; Martínez, J. M.; Pappalardo, R. R.; Sánchez Marcos, E. *J. Chem. Phys.* **2003**, *119*, 6647–6654.
(16) D'Angelo, P.; Migliorati, V.; Mancini, G.; Barone, V.; Chillemi, G. *J. Chem. Phys.* **2008**, *128*, 84502–84508.
(17) Berendsen, H. J. C.; Grigera, J. R.; Straatsma, T. P. *J. Phys. Chem.* **1987**, *91*, 6269–6271.
(18) Mahoney, M. W.; Jorgensen, W. L. *J. Chem. Phys.* **2000**, *112*, 8910–8922.
(19) (a) Tomasi, J.; Mennucci, B.; Cammi, R. *Chem. Rev.* **2005**, *105*, 2999–3093. (b) Cossi, M.; Rega, N.; Scalmani, G.; Barone, V. *J. Chem. Phys.* **2002**, *117*, 43–54. (c) Cossi, M.; Rega, N.; Scalmani, G.; Barone, V. *J. Comput. Chem.* **2003**, *24*, 669–681.
(20) Berendsen, H. J. C.; van der Spool, D.; van Drunen, R. *Comput. Phys. Commun.* **1995**, *91*, 43–56.
(21) Berendsen, H. J. C.; Postma, J. P. M.; Di Nola, A.; Haak, J. R. *J. Chem. Phys.* **1984**, *81*, 3684–3690.
(22) (a) Darden, T.; York, D.; Pedersen, L. *J. Chem. Phys.* **1993**, *98*, 10089–10092. (b) Essmann, U.; Perera, L.; Berkowitz, M. L.; Darden, T.; Lee, H.; Pedersen, L. G. *J. Chem. Phys.* **1995**, *103*, 8577–8592.
(23) van der Spoel, D.; Lindahl, E.; Hess, B.; van Buuren, A. R.; Apol, E.; Meulenhoff, P. J.; Tieleman, D. P.; Sijbers, T. M.; Feenstra, K. A.; van Drunen, R.; Berendsen, H. J. C. Gromacs User Manual, version 3.3. www.gromacs.org (2005).
(24) Hermes, C.; Gilberg, E.; Koch, M. H. *Nucl. Instrum. Methods Phys. Res.* **1984**, *222*, 207–212.
(25) Pettifer, R. F.; Hermes, C. *J. Phys. Colloq.* **1986**, *47*, C8−127.
(26) Pettifer, R. F.; Hermes, C. *J. Appl. Crystallogr.* **1985**, *18*, 404–412.
(27) Filipponi, A.; Di Cicco, A.; Natoli, C. R. *Phys. Rev. B* **1995**, *52*, 15122–15134.
(28) Hedin, L.; Lundqvist, B. I. *J. Phys. C* **1971**, *4*, 2064–2083.
(29) Krause, M. O.; Oliver, J. H. *J. Phys. Chem. Ref. Data* **1979**, *8*, 329–338.
(30) Filipponi, A. *J. Phys. B: At. Mol. Opt. Phys.* **2000**, *33*, 2835–2846.
(31) Kodre, A.; Padešek, J.; Miheliˇc, A.; Arčon, I. *Radiat. Phys. Chem.* **2006**, *75*, 188–194.
(32) Benfatto, M.; Della Longa, S.; Natoli, C. R. *J. Synchrotron Radiat.* **2003**, *10*, 51–57.
(33) Muller, J. E.; Jepsen, O.; Wilkins, J. W. *Solid State Commun.* **1982**, *42*, 365–368.
(34) Chillemi, G.; D'Angelo, P.; Pavel, N. V.; Sanna, N.; Barone, V. *J. Am. Chem. Soc.* **2002**, *124*, 1968–1976.
(35) Egorov, A. V.; Komolkin, A. V.; Lyubartsev, A. P.; Laaksonen, A. *Theor. Chem. Acc.* **2006**, *115*, 170–176.
(36) Lide, D. R. *CRC Handbook of Physics and Chemistry*, 84th ed; CRC Press: Boca Raton, FL, 2003.
(37) Filipponi, A.; Di Cicco, A. *Phys. Rev. B* **1995**, *52*, 15135–5149.

JP806098R